Current Biology, Volume *32*

Supplemental Information

Woodpeckers minimize cranial absorption of shocks

Sam Van Wassenbergh, Erica J. Ortlieb, Maja Mielke, Christine Böhmer, Robert E. Shadwick, and Anick Abourachid

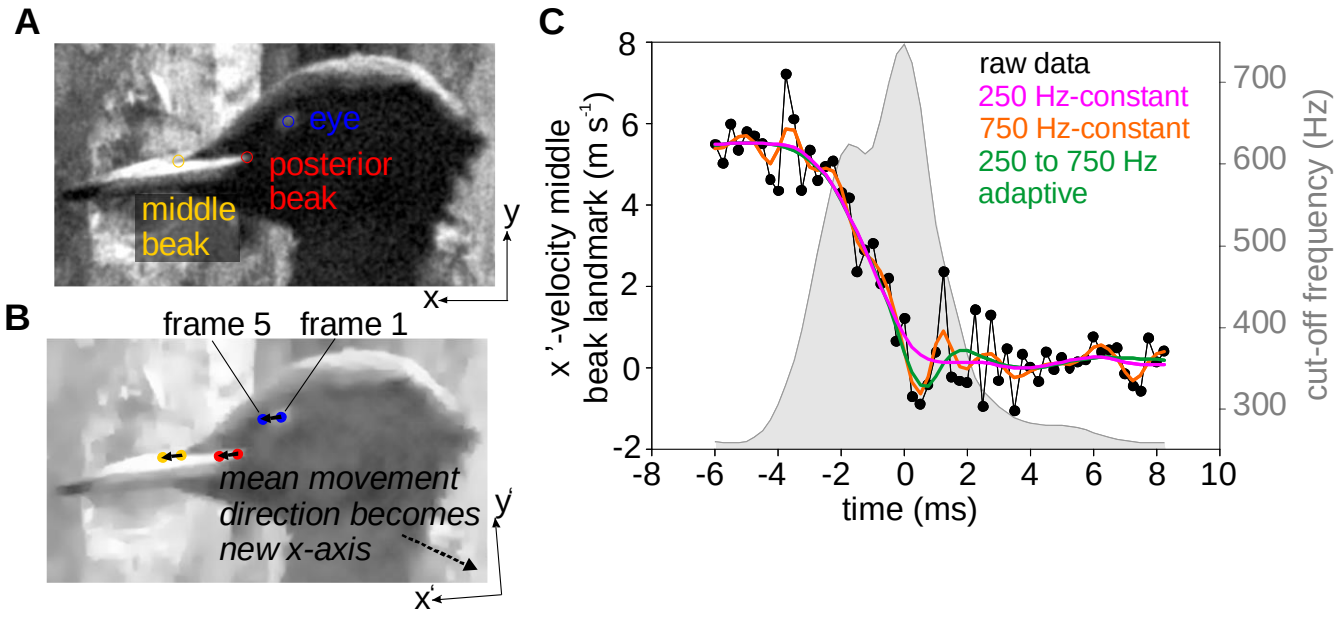

Figure S1. Kinematic analysis protocol (see STAR Methods). Related to Figure 2. A. Position of the three anatomic landmarks that were tracked frame-by-frame for each individual. **B**. Determination of the movement direction as the mean direction vector from frame 1 to frame 5, which is used to rotate the reference frame by aligning new axis x' with this path direction. **C**. Choice of the noise-reduction filter for *D. martius*. While traditional fourth-order Butterworth low-pass filters either caused over-smoothing (cut-off frequency 250 Hz; pink) or did not manage to remove high-frequency velocity fluctuations at the phases of approximate constant velocity (-6 to -4 ms, and 2 to 8 ms) (cut-off frequency 750 Hz; orange), the adaptive filter by Erer had a cut-off frequency (between 250 Hz and 750 Hz) that varied with time (grey curve; right axis scale) and avoided over-smoothing near the time of impact while maintaining sufficient smoothing elsewhere.

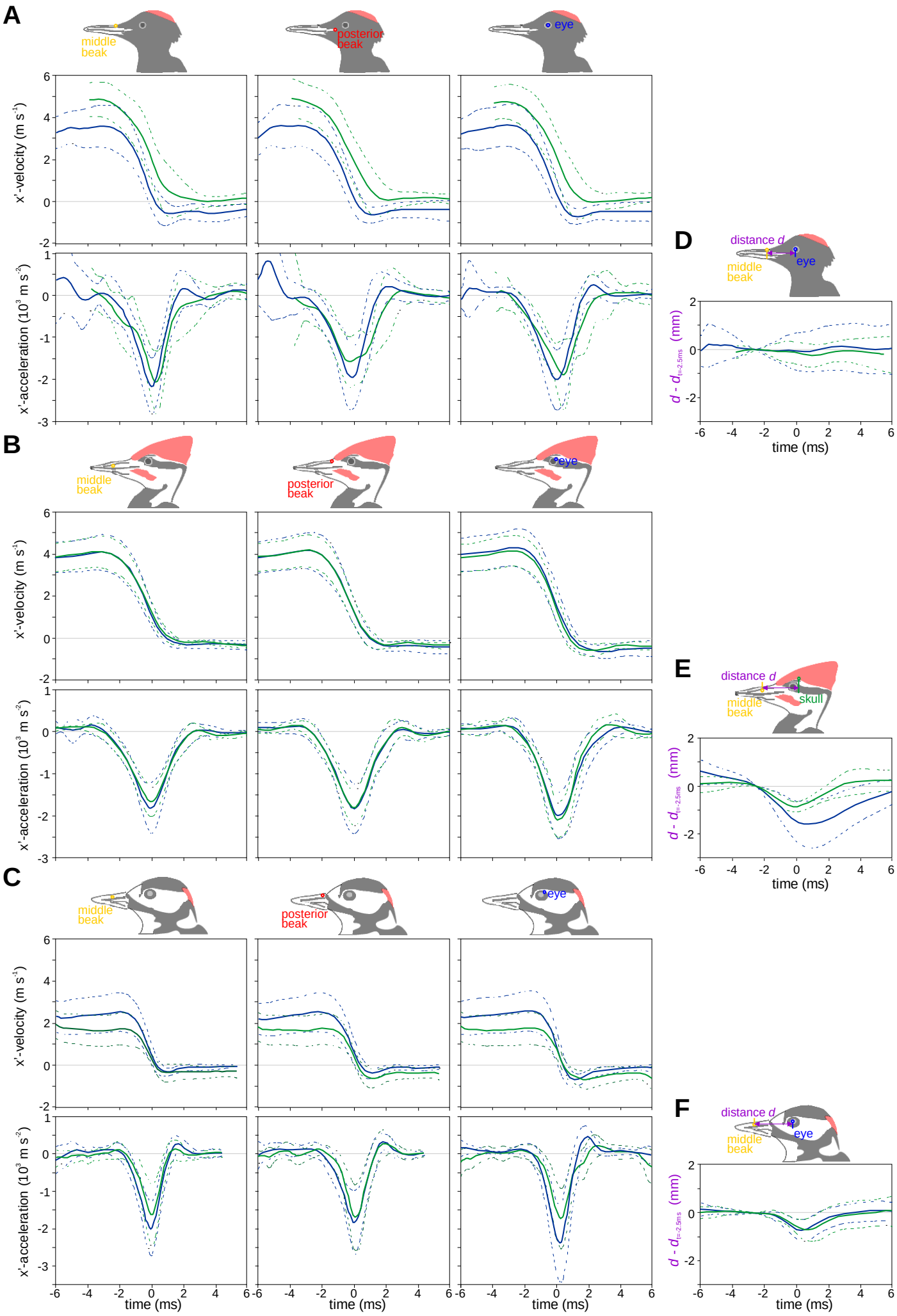
A
middle beak
posterior beak
eye
x'-velocity (m s-1)
x'-acceleration (10³ m s-2)
B
middle beak
posterior beak
eye
x'-velocity (m s-1)
x'-acceleration (10³ m s-2)
C
middle beak
posterior beak
eye
x'-velocity (m s-1)
x'-acceleration (10³ m s-2)
time (ms)
time (ms)
time (ms)
D
distance d
middle beak
eye
d - d t=-2.5ms (mm)
time (ms)
E
distance d
middle beak
skull
d - d t=-2.5ms (mm)
time (ms)
F
distance d
middle beak
eye
d - d t=-2.5ms (mm)
time (ms)

Figure S2. Mean kinematic profiles of pecking in *D. martius* (A, D), *D. pileatus* (B, E), and *D. major* (C, F). Related to Figure 2. (A-C) Time-averaged velocities (upper panels), acceleration (lower panels) from individual 1 (blue; *D. martius N* = 21; *D. pileatus N* = 22; *D. major N* = 22) and individual 2 (green; *D. martius N* = 16; *D. pileatus N* = 9; *D. major N* = 19) are displayed with 95% confidence limits (dashed lines) for the middle beak landmark (left), posterior beak landmark (middle), and eye landmark (right). (D-F) Time-averaged profiles of axial distance change with respect to the value at time -2.5 ms (i.e. just before the start of the beak impact) from individual 1 (blue; *N* as in A-C except for *D. pileatus N* = 15) and individual 2 (green; *N* as in A-C) are displayed with 95% confidence limits (dashed lines). Note that in D-F consistent changes in distance were measured only for *D. pileatus* (1.6 ± 1.0 mm, and 0.85 ± 0.20 mm) and *D. major* (0.73 ± 0.45 mm, and 0.69 ± 0.46 mm) but not in *D. martius*. Time scale in D-F matches that of A-C, with time 0 as the time of peak deceleration of the beak.

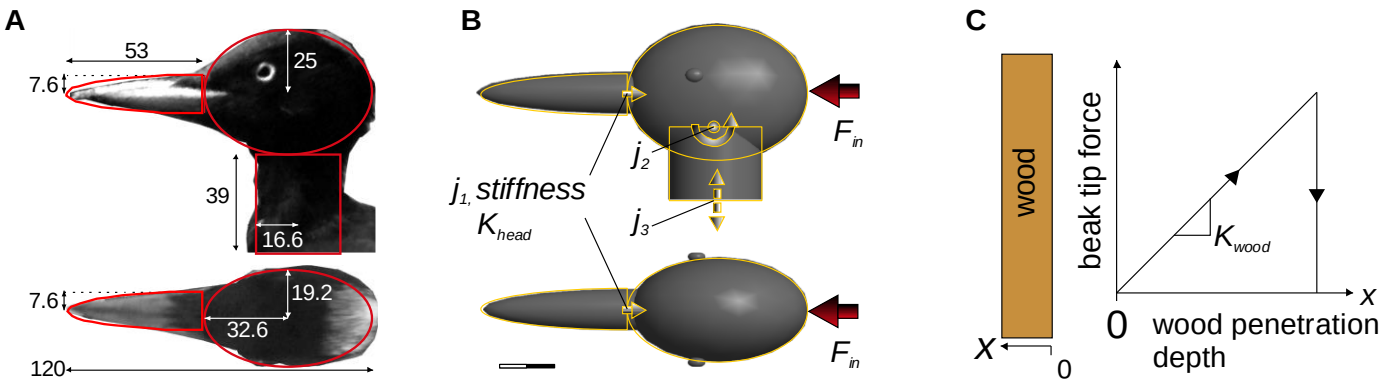

Figure S3. Geometry and boundary conditions of the kinetic model of pecking (see STAR Methods). Related to Figure 3. A. External dimensions (in mm) of the model matching one of the study specimen's image from a lateral view (top) and dorsal view (bottom), with an overlay of the shapes representing the three units: beak, braincase and neck. **B**. Reconstruction of the model geometry with indication of the three joints: j_1, a prismatic joint between the beak and the braincase allowing translation along the horizontal axis. A linear spring with parametrised stiffness K_{head} resists the relative movement of beak and braincase along j_1; j_2, a revolute joint allowing unconstrained rotation in the sagittal plane between braincase and neck; j_3, a prismatic joint allowing unconstrained vertical translation of the base of the neck along an axis fixed in space. Vector F_{in} shows the constant force application point on the braincase. Scale bar equals 2 × 10 mm. **C**. Illustration of the model for wood penetration by the woodpecker's beak. Penetration (from 0 at the wood surface to a certain value along depth axis X) causes a reaction force on the beak increasing linearly with depth. A stiffness constant K_{wood} represents the slope of this relationship. K_{wood} was set to 13000 N m^{-1} to achieve a realistic impact duration and depth. As soon as the beak stops moving deeper into the wood, the reaction force drops to zero.

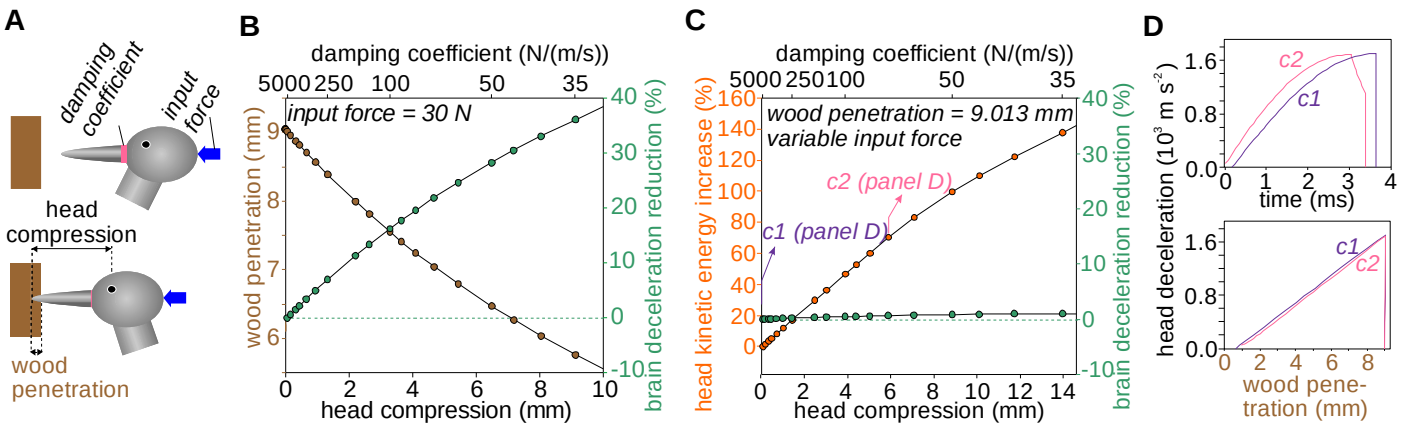

Figure S4. Effect of hypothetical viscous shock damping on pecking performance and braincase deceleration. **Related to Figure 3.** Instead of an elastic tissue absorbing the shock as in Figure 3, the interface between beak and head is simulated here as a dashpot (viscous damping) with a velocity-dependent resistance to compression (magnitude set by the damping coefficient) **A**. The mathematical model's head and neck configuration at the start (top; two model input parameters indicated) and at maximum wood penetration (bottom; two output variables indicated). **B.** Simulations with equal head impulse (constant force input; equal speed at impact) for a range of damping coefficients at the beak-braincase interface (top scale), showing the trade-off between wood penetration depth (brown circles) and brain deceleration reduction relative to the value for maximally stiff crania (green circles). **C**. Simulations achieving equal wood penetration depth by modifying head impulse (input force varies from 30 to 50.84 N; variable speed at impact), showing increasing kinetic energy requirement (orange circles; percentage change relative to maximally stiff crania) when more compression is allowed between beak and braincase. Brain deceleration reduction was always negligible (<0.94%). A comparison of brain deceleration with increasing head compression is further explored for cases *c1* (purple; highest damping coefficient of 5000 N $(m/s)^{-1}$, velocity at impact 3.80 m s^{-1}) and *c2* (pink; damping coefficient 70 N $(m/s)^{-1}$, velocity at impact 4.95 m s^{-1}) in **D,** which shows an equally high peak deceleration of the head compared in *c2* compared to without cranial shock damping, *c1*.

		D. martius		*D. pileatus*		*D. major*	
Δ peak deceleration magnitude		individual 1	individual 2	individual 1	individual 2	individual 1	individual 2
eye to middle beak	*N*	21	16	22	9	22	19
	Δ mean (m s^{-2})	88	-74	223	527	479	141
	95% confidence limit, % of mean beak deceleration	-4.5 to +12.6%	-11.2 to +4.5%	+4.7 to +19.1%	+20.1 to +43.5%	+13.6 to +33.9%	-0.4 to +17.5%
	P (paired t-test)	0.335	0.376	0.002	<0.001	<0.001	0.059
eye to posterior beak	*N*	21	16	22	9	22	19
	Δ mean (m s^{-2})	116	40	169	290	625	-61
	95% confidence limit, % of mean beak deceleration	-1.8 to +12.6%	-12.6 to +16.5%	+4.9 to +12.6%	+7.5 to +23.1%	+21.0 to +42.7%	-11.7 to +5.1%
	P (paired t-test)	0.132(1)	0.781	<0.001	0.002	<0.001	0.418
skull to middle beak	*N*			15	9		
	Δ mean (m s^{-2})			382	388		
	95% confidence limit, % of mean beak deceleration			+8.6 to +34.8%	+10.7 to +36.1%		
	P (paired t-test)			0.003	0.003		
skull to posterior beak	*N*			15	9		
	Δ mean (m s^{-2})			295	151		
	95% confidence limit, % of mean beak deceleration			+5.4 to +26.6%	-4.0 to +20.0%		
	P (paired t-test)			0.006	0.164		

Table S1. Statistical comparison of deceleration magnitudes between head landmarks. Related to Figure 2A. Positive mean difference values denote a higher deceleration magnitude in the eye or skull than in the middle or posterior beak landmark. (1) Normality assumption failed at $P = 0.049$; a Wilcoxon Signed Rank Test shows a significantly higher median of eye deceleration ($Z_{21} = -2.03$; $P = 0.044$).

		D. martius		*D. pileatus*		*D. major*	
peak deceleration magnitude		individual 1	individual 2	individual 1	individual 2	individual 1	individual 2
Eye (Y) *versus* middle beak (X)	*N*	21	16	22	9	22	19
	slope	1.034	0.966	1.118	1.308	1.268	1.07
	95% bootstrapped confidence intervals of slope	0.946 to 1.112	0.891 to 1.033	1.041 to 1.187	1.191 to 1.434	1.206 to 1.349	0.98 to 1.14
	R^2	0.64	0.81	0.71	0.56	0.89	0.862
skull (Y) *versus* middle beak (X)	*N*			12	9		
	slope			1.191	1.232		
	95% bootstrapped confidence intervals of slope			1.088 to 1.318	1.119 to 1.343		
	R^2			0.63	0.57		

Table S2. Between-landmarks Reduced Major Axis regression of peak deceleration magnitudes. Related to Figure 2B.